Engineered 3D-Vessels-on-Chip to study effects of dynamic fluid flow on human induced pluripotent stem cell derived endothelial cells

Graaf, M.N.S. de

Chapter five:

Perfusable Engineered capillary using on-Chip hydrogel guided self-assembly and human iPSC-derived vascular cells

Mees N. S. de Graaf[1*], Dhanesh G. Kasi[1,2*], Francijna E. van den Hil[1], Arn van Maagdenberg[2], Christine L. Mummery[1], Valeria V. Orlova[1]

[1] Department of Anatomy and Embryology, Leiden University Medical Center,

[2] Department of Human Genetics, Leiden University Medical Center

[*]Authors contributed equally

In preparation

Abstract

Realistic models of the human vasculature would benefit understanding of normal physiology and disease pathology in the blood circulatory systems. Here we used a photo patterning system to form near vertical hydrogel walls inside a microfluidic device, generating a perfusable network. The hydrogels had realistic (tissue-like) viscoelastic properties and were permeable to large molecules like 70kD dextran. Endothelial cells from human pluripotent stem cells (hiPSC-ECs) cultured in the hydrogels could be guided to form complex networks. hiPSC-ECs inside channels less than 35 μm diameter adopted a tubular morphology much like capillaries in vivo and did not move up the hydrogel wall and ceiling. By contrast, hiPSC-ECs in 50 μm channels, flattened on the glass substrate and covered the complete hydrogel wall and ceiling. We were able to induce swelling in the engineered vessels, mimicking aspects of vascular pathology. In addition, the hydrogel could be designed to form any shape and a range of widths that encompass a range of vessel types in vivo. Using the methodology developed here, we expect to be able to engineer capillary-networks to investigate the complex interplay between peripheral blood cells, the endothelium and drugs under controlled physiological conditions.

5.1 Introduction

The vasculature is essential for proper organ function and is a key determinant of nutrient and drug distribution[1-3]. Furthermore, blood vessels form the tissue barrier to circulating cells in blood and are thus important for proper inflammatory responses by controlling tissue-barrier permeability and immune cell trafficking[4]. Vessels-on-Chip technology (VoCs) is one way of combining vascular cells in 3D structures resembling blood vessels that support fluidic flow through the lumen. By combining VoCs with biochemical cues like growth factors, extracellular matrix proteins with integrin recognizing-sequences and mechanical stimulation like fluidic flow, synthetic blood vessels with realistic viscoelastic properties can be created[5].

Different methods are being developed to engineer VoC models which include template casting[6-8] and 3D- bioprinting[9]. However, most of these methods are limited in fabrication-resolution and the lumens of the vessels have typically larger diameters (>100 µm) than their *in vivo* equivalents (5-20 µm). For some aspects of vascular modelling, this difference does not limit their use. For example, wall shear stress (WSS) can be easily scaled according to the model diameter by adjusting the flowrate to achieve that required. However, haemodynamic forces at capillary diameters is more complex and not all characteristics can be appropriately recapitulated[10]. One reason is that the luminal diameter of capillary vessels is the same as the diameter of peripheral blood cells. These are then deformed when passing through these capillaries, resulting in haemodynamics that not only depend on continuous fluid flow[11,12]. Due to the complex fluid dynamics, the exact force experienced by the ECs becomes not only dependent on diameter but also on position and haematocrit[13]. Of note, mural-cell interaction involves complete wrapping of the mural cells around the endothelial tube; this cannot be achieved with larger vessels.

Currently, to engineer complex capillary networks in extracellular matrix (ECM), cellular self-assembly is widely used[14-17]. However, these models lack spatial control so that vessels formed vary in diameter which results in haemodynamics that are difficult to control[14]. Furthermore, the majority of vessels thus formed have greater diameters than *in vivo*[14,16]. New methods are therefore being developed to improve the spatial control of capillary network formation.

Scaffold-guided network formation is a potential solution to engineering complex microvascular networks with pre-defined parameters. By using 2-photon Laser ablation[18] or Laser-Based Cavitation[19], small "voids" can be carved inside a hydrogel which can be used to control the size of the model capillary structures. However, for generating complex vascular networks these advanced technologies are time consuming, limiting their scalability. Soft lithography-based approaches allow fabrication of complex capillary-

sized structures inside microfluidic devices[20-22]. These microfluidic networks can be seeded with ECs and can be used for modelling complex haemodynamics. However, the PDMS-channel walls of the microfluidic devices have viscoelastic properties that differ by orders of magnitude from human tissues, affecting how cells experience haemodynamic stimulation nor allow diffusion of drugs or other compounds of interest[23-25].

Guided self-assembly using hydrogel microgrooves(<50 μm) also allows the formation of tubular structures at the capillary scale[26]. Although this approach generates *in vivo* like capillaries in a reproducible and controlled way, they are not perfusable.

To generate perfusable scaffolds that have controllable, in vivo-like viscoelastic properties and are permeable to drugs or other compounds, we propose the Primo photo patterning system (Figure 1). The Primo photopatterning system is small footprint, versatile UV-laser which can be used for 2D-cell patterning[27,28], microfabrication[29] and hydrogel patterning[30]. A key feature of this system is that any pattern can be designed rapidly and optimized with minimal adjustments using any (open-source) graphical software. Furthermore, the controlling software has an advanced stitching algorithm which allows the fabrication of large patterns with minimal stitching artifacts and large microfluidic devices with micrometre-resolution. Furthermore, the system is capable of controlling the intensity of a single pixel which can be used to locally control height or stiffness of the hydrogel[29,30].

We previously reported rapid prototyping of Organ-on-a-Chip (OoC) devices using the primo photopatterning system[29]. In this present work we demonstrated its immediate application by performing controlled hydrogel structuration on-chip using the same setup. (Synthetic) hydrogels with photo-cross linkable functional groups such as gelatin methacryloyl (GelMA) are essential for this approach and these are biocompatible because they provide cell-binding motifs and support enzymatic degradation[31]. Combined with a photo initiator, they allow fabrication of microenvironments that can be chemically and mechanically modified[30]. By employing GelMA and lithium phenyl-2,4,6-trimethylbenzoylphosphinate (LAP) as a photo initiator, scaffolds were produced that could be seeded with cells, perfusable and had capillary dimensions (5-25 μm). Relevant mechanical properties were controlled in microfluidic chips that were 50 μm in height.

The level of control demonstrated here allows engineering of capillary-like vessels that can support *in vitro* modelling of vascular structures. Taken together, our approach opens opportunities for microvascular disease modelling and drug transport studies, since the microfluidic chips can be connected to conventional pumping systems and the microvascular networks are perfusable.

5.2 Results and Discussion

We used the Primo photopatterning-system to fabricate both the microfluidic flow-cells used in this study and hydrogel patterning (Figure 1, S1). Because the master-moulds are fragile, we replicated the cast using an epoxy-resin, which is highly durable and temperature resistant (up to 150 °C) which is ideal for PDMS curing(Figure 1a and b). This method further increased the number of casting moulds that could be produced from a single SU-8 mould. The microfluidic channels have the same footprint previously described as being compatible with future perfusion systems[32]. The gel-reservoir was designed such that the hydrogel could be patterned within 3 frames, minimizing printing time and increasing throughput. Using these dimensions, patterning a single microfluidic channel takes maximally 30 seconds, depending on the required UV-dose(30 mJ/mm^2).

Optimizing the pre-polymer solution

GelMA is widely used as a hydrogel for tissue engineering[31,33]. It is a gelatine-derivative that can be crosslinked using a radical forming photo-initiator and an appropriate light source. Furthermore, it can be mixed with other ECM-components like hyaluronic acid to generate tissue-specific biochemical environments[34]. Different photo-initiators to initiate radical polymerization of the hydrogel. We tested 2 photo-initiators; Lithium phenyl-2,4,6- trimethyl-benzoylphosphinate (LAP, Advanced Biomatrix) and (PLPP, Alveole). Patterning hydrogels using PLPP as photo-initiator showed that a gap formed between the PDMS and the hydrogel due to the oxygen diffusion from the PDMS, ending the radical polymerization (Figure s2)[30]. Because this gap limits hydrogel-PDMS crosslinking, PLPP is not recommended. We, therefore, used LAP instead of PLPP because of its high biocompatibility and water solubility. Moreover, LAP can also be activated using light sources with higher wavelengths (+400 nm) which can potentially be used when cells are incorporated inside the hydrogel as it causes less UV-damage.

To determine a suitable pre-polymer composition, an optimal GelMA-concentration was first determined. The GelMA-concentration ranged from 1%-10% and was first checked for suitability in the protocol. To inject the pre-polymer mixture, it is necessary to warm the solution to 37°C as GelMA solutions have a sol-gel transition between 25-35 °C, depending on their concentration. High concentrations (more than 6%) had a rapid sol-gel transition when removed from the heating block and were therefore considered unsuitable for injection into the microfluidic channels. We then tested the polymerisation of GelMA at concentrations ranging from 1%-5% and varied the UV dose up to 90 mJ/mm^2 and 0.1% LAP, using the Primo photopatterning system. With low concentration (1%) no hydrogel crosslinking was observed. With 2.5% GelMA, defined structures were observed; however these structures were fragile and unsuitable for perfusion (data not shown). Using 5% GelMA, highly defined, flexible structures were

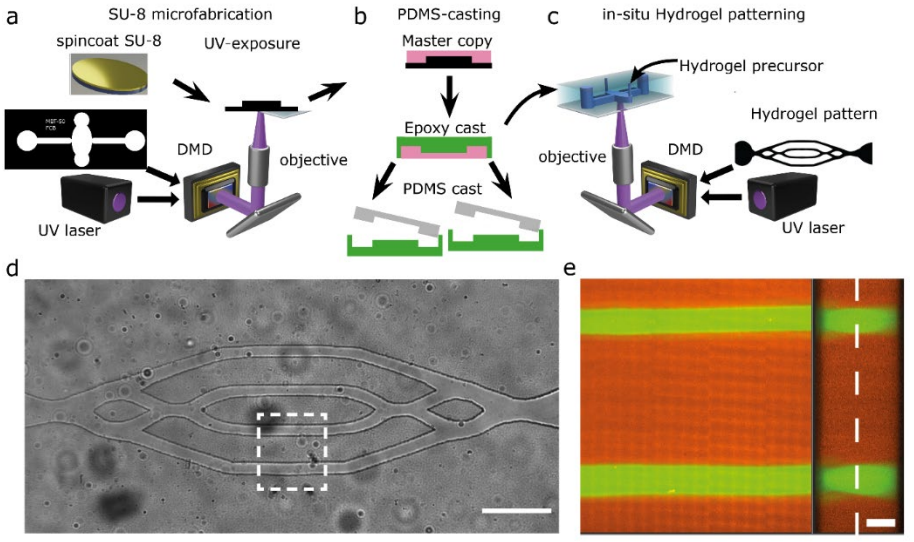

Figure 1: Protocol of hydrogel patterning. (a) *the SU-8 master mould (black) is fabricated using the Primo™ photopatterning system* ***(b)*** *the durable master-copy (pink) is cast from the SU-8 moulds from which multiple identical and durable epoxy moulds (green) can be replicated to increase fabrication throughput from a single design* ***(c)*** *hydrogel patterning is performed using the same setup as microfabrication* ***(d)*** *result of patterned hydrogel immediately after patterning* ***(e)*** *hydrogel incubated with 4 kDa-TRITC(Orange) for 24 hours to image hydrogel; channels were flushed with 70 kDa-FITC(green) to enhance contrast with the fluidic channel; YZ-reconstruction shows near vertical formation of 50 µm height hydrogel scaffolds. Dashed line shows slice of interest.*

formed, that were resilient to high flow rates and pressure. To determine the optimum LAP concentration, concentrations ranging from 0.01%-0.5% were tested at UV doses up to 30 mJ. Concentrations lower than 0.05% did not polymerize but at 0.1%, well-defined structures were visible even with a UV dose as low as 10 mJ/mm^2; this translates to approximately 4 seconds of exposure per frame with the setup and objective used. With higher concentrations of LAP, rapid formation of highly defined structures was observed; however, unwanted crosslinking inside the developing fluidic channels occurred, limiting perfusion. This is due to radical diffusion and at higher concentrations is capable of crosslinking the pre-polymer[35]. Therefore, a LAP concentration 0.1% was considered optimal for this purpose and setup. Using confocal microscopy, we determined that divergence of the optical pathway is minimal within the height of the microfluidic channel and that the hydrogel walls were near-vertical (Figure 1d).

Using the Primo system as we describe, hydrogels with any arbitrary shape can be patterned (Figure 1 d Figure S1b-d). As an example here, we tested a straight channel and a capillary network based on topological optimized with flow-rate equality constraints[36]. By infusing the formed hydrogel with a low molecular weight fluorophore and counter-staining the fluidic channel with heigh-molecular weight dextran the shape of the hydrogel wall can be

imaged using confocal microscopy (Figure 1e). The reconstruction of the Z-stack showed that the hydrogel walls are near-vertical after 24 hours of swelling.

Controlling hydrogel parameters using UV dose.

Next, control of the hydrogel parameters using different UV-doses was determined. First, swelling of the hydrogel structure *in situ* was analysed (Figure 2a). For this, circular structures were patterned using UV doses of 10, 20 and 30 mJ/mm^2 with incubation for 24 hours at 37 °C. The structures measured were compared with the photomasks and the swelling ratio determined (Figure 2a). This showed dose responsive swelling of the GelMA-hydrogel, with 10 mJ/ mm^2 giving the greatest swelling (swelling ratio of 1.2) and 30 mJ /mm^2 shows the smallest ratio (swelling ratio of 1.1). Because the channel width is not an intrinsic property of the hydrogel, we investigated how the channel dimensions are influenced by swelling (Figure 2b). This showed that a reduction of 28 µm in the channel width can be expected when using 10 mJ/mm^2 (Figure 2b and c) a reduction of 14 µm at a dose of 20 mJ/mm^2 and 8 µm at a dose of 30 mJ/mm^2. Because of the high swelling at 10 mJ/mm^2, it is difficult to determine the final channel dimensions exactly and for this reason this was not further investigated.

Determination of diffusion coefficient

To investigate whether the constructed hydrogels allowed compound diffusion, we examined the diffusion of dextran with different molecular weights (Figure 2c). We first patterned a straight channel and perfused it with a mixture of fluorescent dextran compounds (4 kDa, 70 kDa). This mixture was perfused at 1 µl/min using a controlled internal pressure of 20 mbar in the setup described previously to minimize advective transport[32]. By calculating the error function of the intensity profile, the diffusion coefficient can be determined[37]. The diffusion coefficient of 70 kDa dextran for 20 mJ/mm^2 and 30 mJ/mm^2 was respectively 22 ± 2 µm^2/s and 20 ± 2 µm^2/s (Figure 2d), which is similar to values reported previously using hydrogels generated with similar parameters[38]. The diffusion coefficient of 4 kDa for 20 mJ/mm^2 and 30 mJ/mm^2 was 69 ±4 µm^2/s and 63±6 µm^2/s respectively. No reference values were found in literature; however the measured values were as could be expected based on the hydraulic radius and diffusion coefficients in water[39]. Hydrogels with higher UV doses (>60 mJ/mm^2) did not show adequate diffusion (<0.002 µm^2/s based on penetration depth) of the 70 kDa dextran and are thus not recommended for permeability studies (Figure s3). Although the parameters tested demonstrated the utility of the hydrogels, further characterization is needed. Hydrogel stiffness is an important parameter for tissue engineering and the elastic modulus for soft-tissue can range from <1 kPa for brain to 1 MPa for gut or the nerve tissue[25].

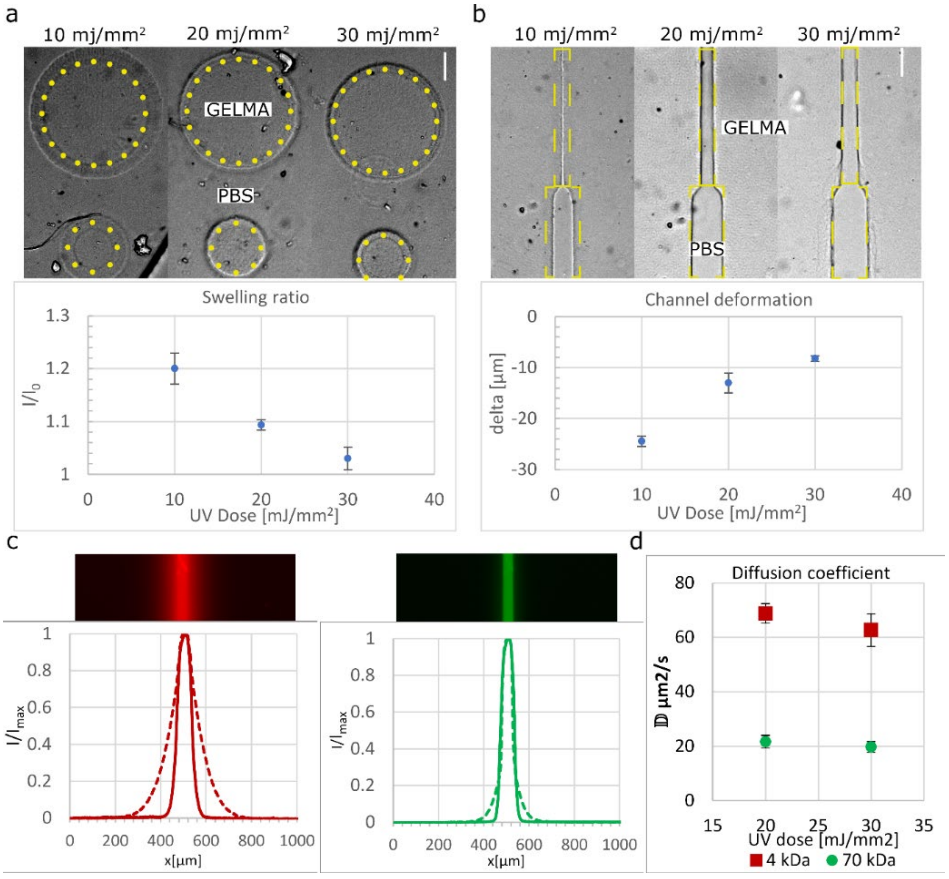

Figure 2: UV-dose related parameters of 5% GelMA and 0.1% LAP. (a) *swelling ratio of 100 and 200 µm hydrogel structures* ***(b)*** *channel deformation resulting from hydrogel swelling* ***(c)*** *4 kDa-TRITC (red) and 70 kDa-FITC (green) dextran diffusion to validate compound permeability (d) Diffusion coefficient of different UV-dose.*

Conditions differing by only 3-fold may alter cell phenotype[40] and therefore accurate determination of mechanical parameters is vital for correct interpretation of experimental data. The stiffness of the construct is dependent on UV-dose, precursor and photo initiator concentration. Although we expected that the hydrogel formed had characteristics similar to *in vivo* (Youngs Modulus of 2 kPa)[41], these parameters still need to be confirmed *in situ,* for example using nanoindentation.

Endothelial cell culture

To examine how vascular cells responded to the engineered scaffolds and test biocompatibility hiPSC-ECs were seeded into the chips using passive pumping (i.e. using the surface tension difference between the 2 mm inlet and 4 mm outlet) to prevent high shear rates and cell damage. In this way, samples could be sequentially seeded although the success rate depended on the quality of the punched inlet.

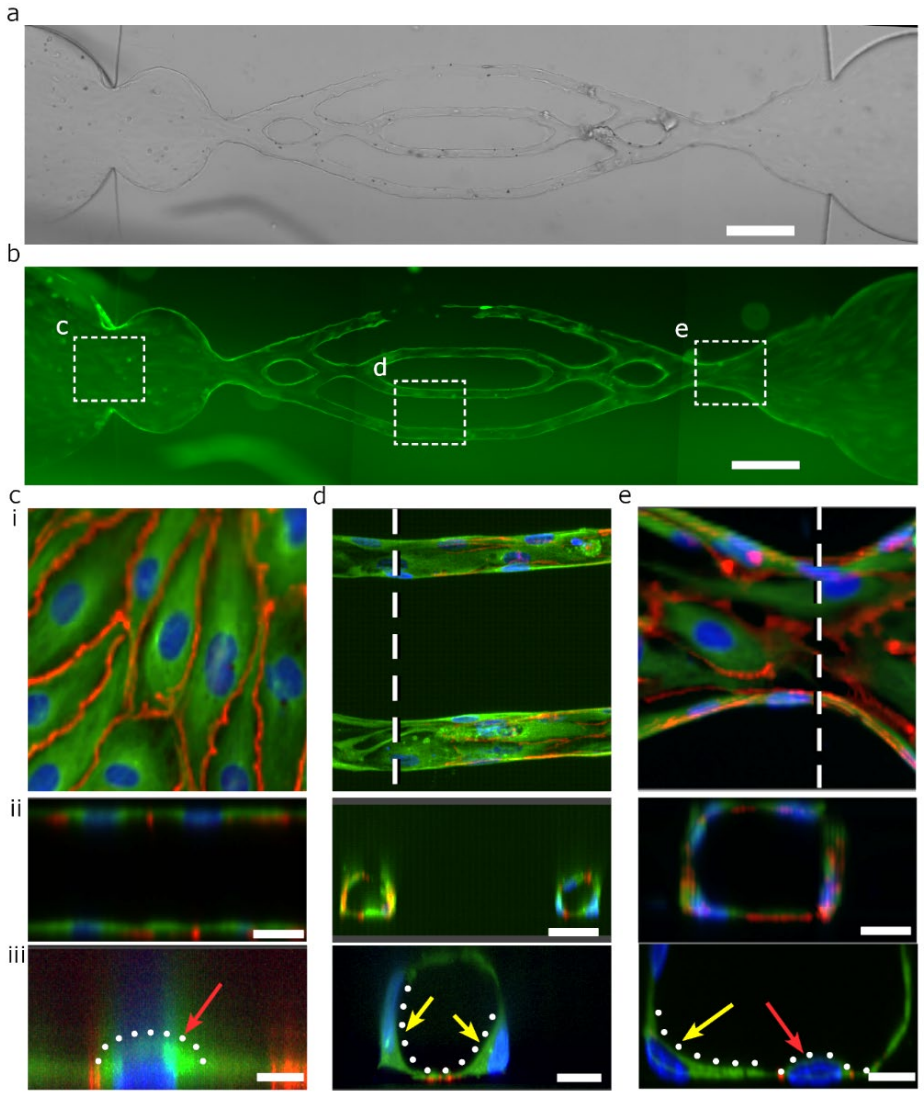

Figure 3: EC-cell culture. (a) *widefield overview of cellularized hydrogel scaffold* ***(b)*** *fluorescent overview of cellularized hydrogel scaffold* ***(c) (i)*** *confocal image of 2D hiPSC-EC monolayer* ***(ii)*** *demonstrating coverage of both ceiling and bottom of the fluidic channel* ***(iii)*** *high magnification of hiPSC-EC monolayer showing a convex nucleus (red arrow)* ***(d)(i)*** *confocal image of capillary part of the hydrogel scaffold,* ***(ii)*** *demonstrating formation of tubular structures inside the hydrogel scaffold* ***(iii)*** *high magnification of capillary structures showing concave cell nuclei (yellow arrows) where the cell body is preferably situated in the corner of the small channel* ***(e) (i)*** *confocal image of the outlet of the hydrogel scaffold* ***(ii)*** *showing hiPSC-EC monolayer formation of the hydrogel sidewall and ceiling in the fluidic device* ***(iii)*** *high magnification of wider hydrogel scaffold shows a combination of concave nuclei (yellow arrow) and convex nuclei (red arrow) Scalebars: a,b 200 µm, c,d,e i,ii 20 µm Scalebars iii 10 µm. Green: TUBA1B-mEGFP, Blue: Nuclei, Red: VE-cadherin****.***

Confocal microscopy was used to examine the hiPSC-ECs in greater detail. This revealed that hiPSC-ECs in wide structures (>50 µm) formed confluent monolayers covering both walls and ceilings, much as in conventional 2D flow channels. However, when the channel width was smaller than 35 µm, the hiPSC-ECs formed tubular structures resembling a capillary. Moreover, these tubular structures appeared symmetric, with the same height as width of the vessel. Exploiting this property allowed engineering of luminal diameters as small as 10 µm. Within the microfluidic channel these capillary structures were also fully perfusable. Interestingly, within self-assembled tubular structures, the nucleus of the hiPSC-ECs was located preferably on the side of the hydrogel channel and cross sections of the nuclei appeared concave (Figure 4b), similar to those in capillaries *in vivo* [42] but in contrast to normal planar-cell cultures were the nucleus is convex and within the flow field (Figure 4a). The nucleus has a significant amount of hydrodynamic drag and this can alter cell polarity and the EC-phenotype[43]. In contrast to our observation in hiPSC-ECs, Human Umbilical Vein ECs (HUVECs) cultured in 30x30 µm PDMS- channels retained a monolayer morphology[22]. Whether the change in nuclear morphology in hiPSC-ECs results in functional differences remains to be investigated.

5.3 Limitations of the presented System

Despite the advantages of the system we described here, it still has some limitations. Firstly, cell seeding is not optimal, as the required inlet/outlet combination for sufficient pressure required large punched holes which resulted in large reservoirs where cells tended to accumulate. Therefore, the use of an optimized Fluidic Circuit Board is recommended to automate cell seeding steps[44]. The capillary network here was designed on the assumption that the hiPSC-ECs would grow vertically on the wall. However, because the cells formed small tubular structures, the shear rates were significantly larger than expected. Therefore, other designs should be considered with a higher number of capillary-like structures to lower the shear rate (figure s1d).

5.4 Conclusion

Using a DMD photo patterning system, we were able to form near vertical hydrogel walls inside a microfluidic device, generating a perfusable network. The hydrogels had realistic (tissue-like) viscoelastic properties compared to PDMS or cell culture plastic and were permeable to large molecules like 70 kD dextran which would make them suitable for drug transport experiments. hiPSC-ECs cultured could be guided to form complex networks in the hydrogels. We found that hiPSC-ECs inside channels less than 35 µm, hiPSC-ECs adopted an *in vivo*-like capillary morphology. They did not move up the hydrogel wall and ceiling. hiPSC-ECs in 50 µm channels, flattened on the glass substrate and covered the complete hydrogel wall and ceiling. Using the methodology developed here, it might be possible to engineer a capillary-

network which can be used to investigate the complex interplay between peripheral blood cells and the endothelium under controlled physiological conditions.

5.5 Materials and Methods

Mask-less photolithography to generate the microfluidic device master mould

Glass substrates containing SU-8 microstructures were used as master-moulds and were fabricated as previously described (Figure 1a)[29]. Briefly, glass substrates coated with a 50 µm thick SU-8-2075 (Kayaku Advanced Materials, Inc) were placed into an adjustable microscope holder for backside UV exposure. A mask-less DMD-based photolithography system (PRIMO, Alvéole) connected to a Leica DMi8 inverted microscope with motorized stage was used for exposure. Binary digital photomasks were designed in an open-source vector graphics editor (Inkscape) according to manufacturers' instructions. Digital photomasks were then loaded into the Leonardo software (Alvéole) and projected by the system onto the substrate via a 5X/0.15NA objective using a 6 mJ/mm2 laser dose. Finally, post-exposure bake and subsequent development of SU-8 were performed according to manufacturers' instructions.

Mould replication and Soft Lithography

The SU-8 master-mould was replicated by first generating a master-copy followed by replication to make durable epoxy-resin copies (Figure 1b). This SU-8 master-mould was laminated in 60 mm diameter polystyrene Petri dishes (Greiner Bio-One, Frickenhausen, Germany) using a thin layer of Polydimethylsiloxane (PDMS, sylgard 184, DOW), after which a master copy was made using Smooth-Sil 940 (Smooth-On) according to manufacturers' instructions. Smooth-Sil 940 components were mixed and degassed for 30 min at RT under high vacuum. 10 g was poured into the Petri dish and cured at RT for 24 hours. The Smooth-Sil 940 was then "demoulded" from the Petri dish by carefully cutting a 35 mm circle around the microstructures using a scalpel. Next, the master copies were mounted in a polypropylene cover lid and casted with EpoxAcast 670 HT (Smooth-on). EpoxAcast components were mixed with thinner (100: 17.6:10, A:B:thinner) to reduce resin viscosity according to manufacturers' instructions and degassed at RT for 30 min under high vacuum. The mixture was cast and placed in a sonication bath for 5 min to remove all air bubbles from the structures. After sonication the cast was cured at RT for 24 hours followed by 2 hours at 60 °C and 20 hours at 80 °C. The resulting epoxy moulds were then used for soft lithography to make PDMS chips. Briefly, PDMS was mixed in a 10:1 (base:curing agent) mass ratio and degassed for 30 min at RT, dispensed over the epoxy-moulds and placed at 60 °C. After curing, PDMS was coold to RT, then the PDMS was gently peeled off. The inlets of the fluidic channels were punched using a 2

mm biopsy puncher. For the outlets, a 4 mm biopsy puncher was used and for the inlets, a 1 mm biopsy puncher.

Chemical functionalization of microfluidic channels

Prepared microfluidic devices and coverslips were treated with air plasma (50 KHz, 50 W) for 1 min (CUTE, Femto Science Inc.,Gyeonggi-do, Korea), after which the devices were contact bonded onto the glass coverslips. Fluidic channels were then immediately functionalized to covalently bind the hydrogel to the channel wall. Briefly, a stock solution containing 47.5 % (3-Aminopropyl)triethoxysilane (APTES, sigma) , 50 % methanol(technical grade, Sigma) and 2.5 % distilled water(Gibco) (% v/v) was prepared. The stock solution was then diluted 1:500 to obtain a working solution with a final APTES concentration of 0.095%. The diluted APTES solution was injected in the microfluidic channels and the Petri dish sealed with Parafilm followed by 40 min incubation at RT. A reservoir of 10 ml methanol was included in the closed Petri dish to prevent methanol evaporation. The microfluidic channels were then washed with methanol, dried using a stream of clean dry air (CDA) and baked on a hotplate set at 110 °C for 30 min. 1 % glutaraldehyde solution (v/v) was then injected and the microfluidic devices incubated for 30 min after which they were flushed with distilled water and dried using a stream of CDA.

Hydrogel patterning

All of the following steps up to cell seeding were performed in a room where lighting was filtered using LITHOPROTECT® UV-filter (Litoprotect) to prevent any unwanted crosslinking. 10% gelatin methacryloyl (GelMA, Bloom 300, Sigma-Aldrich) in phosphate-buffered saline (PBS) (w/v) was filtered using a 0.2 µm Puradisc syringe filter (Whatman), aliquoted and stored at 4 °C. Before using, the solution was pre-warmed to 37 °C and mixed 1:1 with freshly prepared and filtered 0.2 % lithium phenyl-2,4,6 trimethylbenzoylphosphinate (LAP, Sigma-Aldrich) in PBS solution (w/v) to obtain a hydrogel working solution containing 5 % GelMA and 0.1 % LAP. Finally, the working solution was prewarmed to 37 °C and 3 µL was injected into the gel chambers of the prewarmed microfluidic devices. The filled microfluidic devices were immediately placed into an adjustable microscope holder for exposure using the DMD-based system (PRIMO, Alvéole, France). A digital photomask containing the GelMA scaffold pattern was designed in Inkscape, loaded into Leonardo (Alvéole) and projected by the system onto the microfluidic device gel chamber via a 5X/0.15NA objective using the specified laser dose. Microfluidic devices were then flushed using a prewarmed syringe with PBS without Ca^{2+} and Mg^{2+} (PBS-) to remove non-crosslinked GelMA and excess photo initiator.

To promote later cell adhesion, chips were incubated with a filtered fibronectin solution (10 µg/ml, bovine, Thermo Fisher Scientific) for 30 min,

flushed with cell culture medium (EGM-2) and finally incubated at 37 °C until cell seeding.

Determination of hydrogel swelling ratio

A digital photomask containing circular patterns of 100 and 200 µm in diameter was designed in Inkscape and projected using the PRIMO system at laser doses of 10, 20 and 30 mJ/mm^2 using the Leonardo software (Alvéole) and prepared as described above. The microfluidic devices were flushed with EC growth medium (EGM-2) and placed inside an incubator at 37 °C for 24 hours. After incubation, the structured hydrogels inside the devices were imaged using an EVOS M7000 microscope (ThermoFisher Scientific) and compared to the dimensions of the digital photomask. Similarly, straight fluidic channels 30 and 60 µm in width (Figure s1b) were patterned and flushed as described above. After 24 hrs incubation, the hydrogel channels were imaged and compared to the dimensions on the digital photomask.

Determination of diffusion coefficient

Straight channels (60 and 30) µm in width (Figure s1b) were generated as described above using a 20 and 30 mJ/mm^2 laser dose. EGM2 was supplemented with 4-kDa TRITC-dextran (0.03 mg/ml, 7.1 µM) and 70-kDa FITC-dextran (0.5 mg/ml, 7.1 µM). Microfluidic devices were individually connected to a custom designed perfusion system (Fluigent) controlled as previously described[32], with an internal pressure lower than 20 mbar to limit advective transport towards the gel during perfusion. Devices were placed on an EVOS M7000 microscope (ThermoFisher Scientific) and sequential images were obtained at an interval of 15 seconds for 10 min. Images were analysed using a custom python script to determine the diffusion coefficient by fitting the error function on the intensity profile, as described elsewhere[37]. The average of the first 5 timepoints was used as the diffusion coefficient.

Differentiation and expansion of hiPSC-ECs

Alpha-tubulin- monomeric Enhanced Green Fluorescent Protein-hiPSCs (TUBA1B-mEGFP, Cell Line ID: AICS-0012 cl.105, https://hpscreg.eu/cell-line/UCSFi001-A-2) were obtained from the Allen institute[45]. hiPSC-ECs were differentiated as previously described[46]. Briefly, TUBA1B-mEGFP-hiPSCs were maintained in TeSR™-E8™ medium on vitronectin-coated 6-well plates and seeded at day (-1). Twenty-four hours after seeding, E8 medium was replaced with B(P)EL medium supplemented with 8 µM CHIR. On day 3, the medium was replaced with B(P)EL medium supplemented with 50 ng/ml VEGF (R&D systems) and 10 µM SB431542 (Tocris Bioscience); cells were refreshed with the same medium on days 7 and 9. hiPSC-ECs were isolated on day 10 using CD31-Dynabeads™ (Invitrogen), expanded for 3 days and cryopreserved. hiPSC-ECs from cryo-preserved batches were used in all experiments. They were thawed and expanded in Endothelial Cell-Serum Free

Medium (EC-SFM, Gibco, cat. No. 11111-044) supplemented with 1 % human platelet poor serum, FGF2 (20 ng/mL) and VEGF (30 ng/mL), on a 0.1 % gelatine-coated T-75 culture flask. hiPSC-ECs were used at passage 2 for all experiments.

Seeding of scaffolds with hiPSC-ECs

hiPSC-ECs were harvested using TrypLE™ (ThermoFisher Scientific) and resuspended at a concentration of $15x10^6$ cells/ml in EGM-2 supplemented with 50 ng/mL VEGF and PenStrep(25 Units/ml). 2 µl of cell suspension was carefully pipetted on to the bottom of the inlet (2 mm) using gel-loader pipette tips and cells traversed the microfluidic channels via passive pumping. Once cells were stationary, medium was pipetted into the outlet and cells were incubated for 2 days. Medium was refreshed twice a day using passive pumping.

Live cell staining and microscopy

hiPSC-ECs were in culture for 48 hours on the patterned hydrogels. Prior to imaging, 10 µl of EGM-2 with anti-VE-cadherin (CD144-mouse anti-Human Alexa-647, BD Bioscience, diluted 1:200) and Hoechst—33342 (ThermoFischer Scientific, 1 µg /ml) was injected into the microfluidic devices and incubated for 30 min at 37 °C. Next, medium was refreshed and samples were imaged using Leica DMi8 microscope equipped with a Dragonfly® spinning disk (pinhole:20 µm) (Andor). A HC PL APO 20x/0.75 IMM CORR CS2 objective was used with water as immersion medium. This objective was combined with 2x camera magnification to enhance lateral resolution. An iXon CCD camera was used to record the signal. Details of the capillary bed were imaged using 63x or 100x objectives using oil as immersion medium and a pinhole of 40 µm.

Supplementary materials

See Supplementary materials for additional figures of design masks, PLPP based crosslinking, high UV-dose permeability and EC sprout-formation.

References

1 Glassman, P. M. *et al.* Targeting drug delivery in the vascular system: Focus on endothelium. *Adv Drug Deliv Rev* **157**, 96-117, doi:10.1016/j.addr.2020.06.013 (2020).

2 Reiterer, M. & Branco, C. M. Endothelial cells and organ function: applications and implications of understanding unique and reciprocal remodelling. *Febs J* **287**, 1088-1100, doi:10.1111/febs.15143 (2020).

3 Urbanczyk, M., Zbinden, A. & Schenke-Layland, K. Organ-specific endothelial cell heterogenicity and its impact on regenerative medicine and biomedical engineering applications. *Adv Drug Deliv Rev* **186**, 114323, doi:10.1016/j.addr.2022.114323 (2022).

4 Muller, W. A. Leukocyte-endothelial-cell interactions in leukocyte transmigration and the inflammatory response. *Trends Immunol* **24**, 327-334, doi:10.1016/s1471-4906(03)00117-0 (2003).

5 James, B. D. & Allen, J. B. Vascular Endothelial Cell Behavior in Complex Mechanical Microenvironments. *Acs Biomater Sci Eng* **4**, 3818-3842, doi:10.1021/acsbiomaterials.8b00628 (2018).

6 Chrobak, K. M., Potter, D. R. & Tien, J. Formation of perfused, functional microvascular tubes in vitro. *Microvasc Res* **71**, 185-196, doi:10.1016/j.mvr.2006.02.005 (2006).

7 Jimenez-Torres, J. A., Peery, S. L., Sung, K. E. & Beebe, D. J. LumeNEXT: A Practical Method to Pattern Luminal Structures in ECM Gels. *Adv Healthc Mater* **5**, 198-204, doi:10.1002/adhm.201500608 (2016).

8 Polacheck, W. J., Kutys, M. L., Tefft, J. B. & Chen, C. S. Microfabricated blood vessels for modeling the vascular transport barrier. *Nat Protoc* **14**, 1425-1454, doi:10.1038/s41596-019-0144-8 (2019).

9 Kolesky, D. B. *et al.* 3D bioprinting of vascularized, heterogeneous cell-laden tissue constructs. *Adv Mater* **26**, 3124-3130, doi:10.1002/adma.201305506 (2014).

10 Ebrahimi, S. & Bagchi, P. A computational study of red blood cell deformability effect on hemodynamic alteration in capillary vessel networks. *Sci Rep* **12**, 4304, doi:10.1038/s41598-022-08357-z (2022).

11 Secomb, T. W., Hsu, R. & Pries, A. R. Motion of red blood cells in a capillary with an endothelial surface layer: effect of flow velocity. *Am J Physiol Heart Circ Physiol* **281**, H629-636, doi:10.1152/ajpheart.2001.281.2.H629 (2001).

12 Hogan, B., Shen, Z., Zhang, H., Misbah, C. & Barakat, A. I. Shear stress in the microvasculature: influence of red blood cell morphology and endothelial wall undulation. *Biomech Model Mechanobiol* **18**, 1095-1109, doi:10.1007/s10237-019-01130-8 (2019).

13 Ascolese, M., Farina, A. & Fasano, A. The Fahraeus-Lindqvist effect in small blood vessels: how does it help the heart? *J Biol Phys* **45**, 379-394, doi:10.1007/s10867-019-09534-4 (2019).

14 Kim, S., Lee, H., Chung, M. & Jeon, N. L. Engineering of functional, perfusable 3D microvascular networks on a chip. *Lab Chip* **13**, 1489-1500, doi:10.1039/c3lc41320a (2013).

15 Adriani, G., Ma, D., Pavesi, A., Kamm, R. D. & Goh, E. L. A 3D neurovascular microfluidic model consisting of neurons, astrocytes and cerebral endothelial cells as a blood-brain barrier. *Lab Chip* **17**, 448-459, doi:10.1039/c6lc00638h (2017).

16 Wan, Z. *et al.* A Robust Method for Perfusable Microvascular Network Formation In Vitro. *Small Methods* **6**, e2200143, doi:10.1002/smtd.202200143 (2022).

17 Phan, D. T. T. *et al.* A vascularized and perfused organ-on-a-chip platform for large-scale drug screening applications. *Lab Chip* **17**, 511-520, doi:10.1039/c6lc01422d (2017).

18 Arakawa, C. *et al.* Biophysical and biomolecular interactions of malaria-infected erythrocytes in engineered human capillaries. *Sci Adv* **6**, eaay7243, doi:10.1126/sciadv.aay7243 (2020).

19 Enrico, A. *et al.* 3D Microvascularized Tissue Models by Laser-Based Cavitation Molding of Collagen. *Adv Mater* **34**, e2109823, doi:10.1002/adma.202109823 (2022).

20 Fenech, M. *et al.* Microfluidic blood vasculature replicas using backside lithography. *Lab Chip* **19**, 2096-2106, doi:10.1039/c9lc00254e (2019).

21 Tsai, M. *et al.* In vitro modeling of the microvascular occlusion and thrombosis that occur in hematologic diseases using microfluidic technology. *J Clin Invest* **122**, 408-418, doi:10.1172/JCI58753 (2012).

22 Tsvirkun, D., Grichine, A., Duperray, A., Misbah, C. & Bureau, L. Microvasculature on a chip: study of the Endothelial Surface Layer and the flow structure of Red Blood Cells. *Sci Rep* **7**, 45036, doi:10.1038/srep45036 (2017).

23 Deguchi, S., Hotta, J., Yokoyama, S. & Matsui, T. S. Viscoelastic and optical properties of four different PDMS polymers. *J Micromech Microeng* **25**, doi:10.1088/0960-1317/25/9/097002 (2015).

24 Johnston, I. D., McCluskey, D. K., Tan, C. K. L. & Tracey, M. C. Mechanical characterization of bulk Sylgard 184 for microfluidics and microengineering. *J Micromech Microeng* **24**, doi:10.1088/0960-1317/24/3/035017 (2014).

25 Guimarães, C. F., Gasperini, L., Marques, A. P. & Reis, R. L. The stiffness of living tissues and its implications for tissue engineering. *Nat Rev Mater* **5**, 351-370, doi:10.1038/s41578-019-0169-1 (2020).

26 Jiang, L. Y. & Luo, Y. Guided assembly of endothelial cells on hydrogel matrices patterned with microgrooves: a basic model for microvessel engineering. *Soft Matter* **9**, 1113-1121, doi:10.1039/c2sm27126e (2013).

27 Delepine, C. *et al.* Altered microtubule dynamics and vesicular transport in mouse and human MeCP2-deficient astrocytes. *Hum Mol Genet* **25**, 146-157, doi:10.1093/hmg/ddv464 (2016).

28 Strale, P. O. *et al.* Multiprotein Printing by Light-Induced Molecular Adsorption. *Adv Mater* **28**, 2024-2029, doi:10.1002/adma.201504154 (2016).

29 Kasi, D. G. *et al.* Rapid Prototyping of Organ-on-a-Chip Devices Using Maskless Photolithography. *Micromachines (Basel)* **13**, doi:10.3390/mi13010049 (2021).

30 Pasturel, A., Strale, P. O. & Studer, V. Tailoring Common Hydrogels into 3D Cell Culture Templates. *Adv Healthc Mater* **9**, e2000519, doi:10.1002/adhm.202000519 (2020).

31 Bupphathong, S. *et al.* Gelatin Methacrylate Hydrogel for Tissue Engineering Applications-A Review on Material Modifications. *Pharmaceuticals (Basel)* **15**, doi:10.3390/ph15020171 (2022).

32 de Graaf, M. N. S., Vivas, A., van der Meer, A. D., Mummery, C. L. & Orlova, V. V. Pressure-Driven Perfusion System to Control, Multiplex and Recirculate Cell Culture Medium for Organs-on-Chips. *Micromachines (Basel)* **13**, 1359, doi:10.3390/mi13081359 (2022).

33 Xiao, S. *et al.* Gelatin Methacrylate (GelMA)-Based Hydrogels for Cell Transplantation: an Effective Strategy for Tissue Engineering. *Stem Cell Rev Rep* **15**, 664-679, doi:10.1007/s12015-019-09893-4 (2019).

34 Skardal, A. *et al.* Photocrosslinkable hyaluronan-gelatin hydrogels for two-step bioprinting. *Tissue Eng Part A* **16**, 2675-2685, doi:10.1089/ten.TEA.2009.0798 (2010).

35 LeValley, P. J. *et al.* Fabrication of Functional Biomaterial Microstructures by in Situ Photopolymerization and Photodegradation. *Acs Biomater Sci Eng* **4**, 3078-3087, doi:10.1021/acsbiomaterials.8b00350 (2018).

36 Liu, Z. Y., Gao, Q. Y., Zhang, P., Xuan, M. & Wu, Y. H. Topology optimization of fluid channels with flow rate equality constraints. *Struct Multidiscip O* **44**, 31-37, doi:10.1007/s00158-010-0591-x (2011).

37 Park, G. Y. Diffusion coefficient calculated by complementary error function for the sublimation diffusion of disperse dye (vol 14, pg 1, 2019). *J Eng Fiber Fabr* **15**, doi:10.1177/1558925019885200 (2020).

38 Kaemmerer, E. *et al.* Gelatine methacrylamide-based hydrogels: an alternative three-dimensional cancer cell culture system. *Acta Biomater* **10**, 2551-2562, doi:10.1016/j.actbio.2014.02.035 (2014).

39 Silva, J. V., Peixoto, P. D., Lortal, S. & Floury, J. Transport phenomena in a model cheese: the influence of the charge and shape of solutes on diffusion. *J Dairy Sci* **96**, 6186-6198, doi:10.3168/jds.2013-6552 (2013).

40 Shen, Y. *et al.* Reduction of Liver Metastasis Stiffness Improves Response to Bevacizumab in Metastatic Colorectal Cancer. *Cancer Cell* **37**, 800-817.e807, doi:10.1016/j.ccell.2020.05.005 (2020).

41 Yin, J., Yan, M., Wang, Y., Fu, J. & Suo, H. 3D Bioprinting of Low-Concentration Cell-Laden Gelatin Methacrylate (GelMA) Bioinks with a Two-Step Cross-linking Strategy. *ACS Appl Mater Interfaces* **10**, 6849-6857, doi:10.1021/acsami.7b16059 (2018).

42 Nahirney, P. C. & Tremblay, M. E. Brain Ultrastructure: Putting the Pieces Together. *Front Cell Dev Biol* **9**, 629503, doi:10.3389/fcell.2021.629503 (2021).

43 Tkachenko, E. *et al.* The nucleus of endothelial cell as a sensor of blood flow direction. *Biol Open* **2**, 1007-1012, doi:10.1242/bio.20134622 (2013).

44 Vollertsen, A. R. *et al.* Modular operation of microfluidic chips for highly parallelized cell culture and liquid dosing via a fluidic circuit board. *Microsyst Nanoeng* **6**, 107, doi:10.1038/s41378-020-00216-z (2020).

45 Roberts, B. *et al.* Systematic gene tagging using CRISPR/Cas9 in human stem cells to illuminate cell organization. *Mol Biol Cell* **28**, 2854-2874, doi:10.1091/mbc.E17-03-0209 (2017).

46 Orlova, V. V. *et al.* Generation, expansion and functional analysis of endothelial cells and pericytes derived from human pluripotent stem cells. *Nat Protoc* **9**, 1514-1531, doi:10.1038/nprot.2014.102 (2014).

Chapter five: Supplementary materials

Perfusable Engineered capillary bed using on-Chip hydrogel guided self-assembly and iPSC derived vascular cells

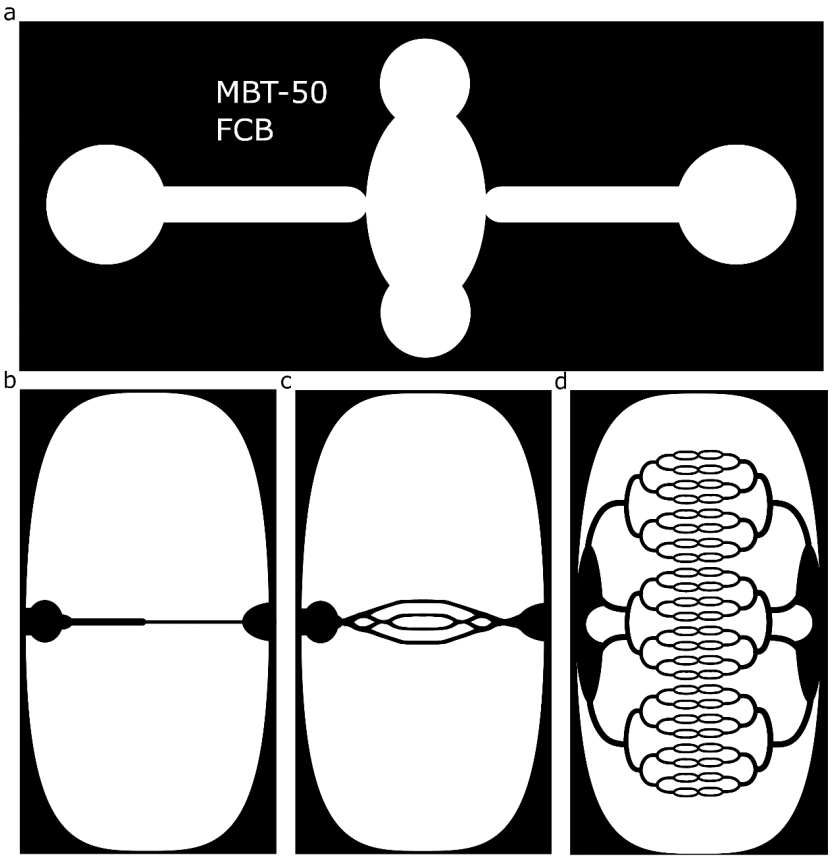

Figure S1: Used patterns for this study. (a) *microfluidic channel* ***(b)*** *straight channels* ***(c)*** *topological optimized capillary network* ***(d)*** *proposed high density capillary network*

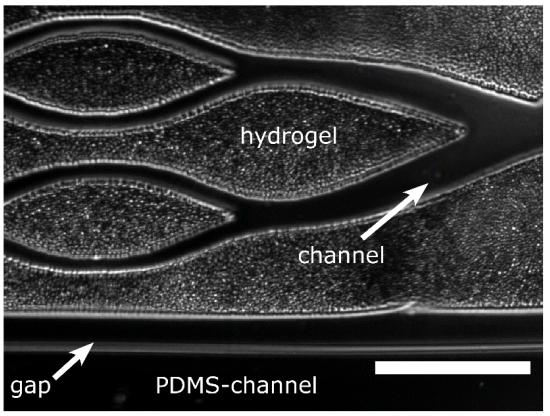

***Figure S2: Hydrogel patterning with PLPP**. a gap is visible between hydrogel and PDMS- side wall. Scale bar is 200µm*

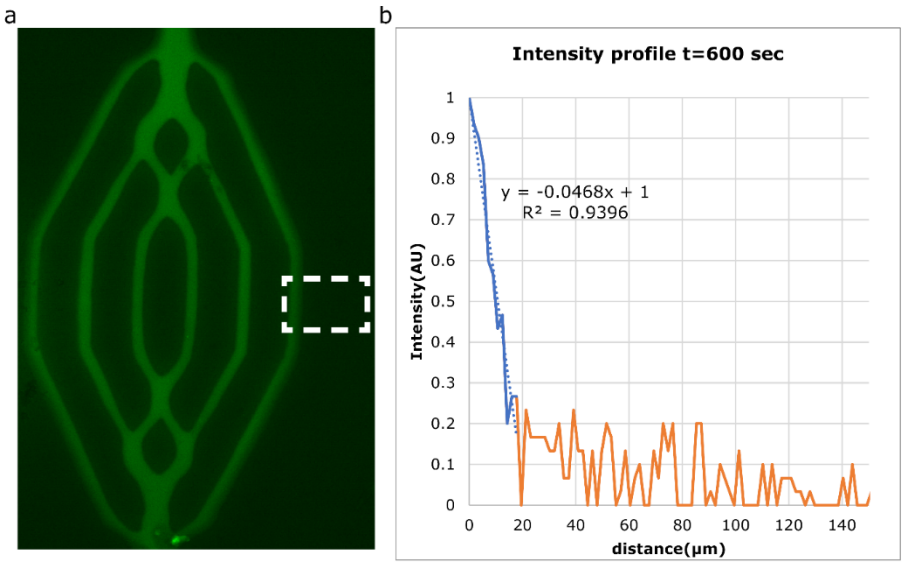

***Figure S3: Permeability of 70kDa in hydro gel patterned with 60 mj/mm²**. Analyses shows minimal penetration of the fluorescent dextran and accompanied low diffusion coefficient.*

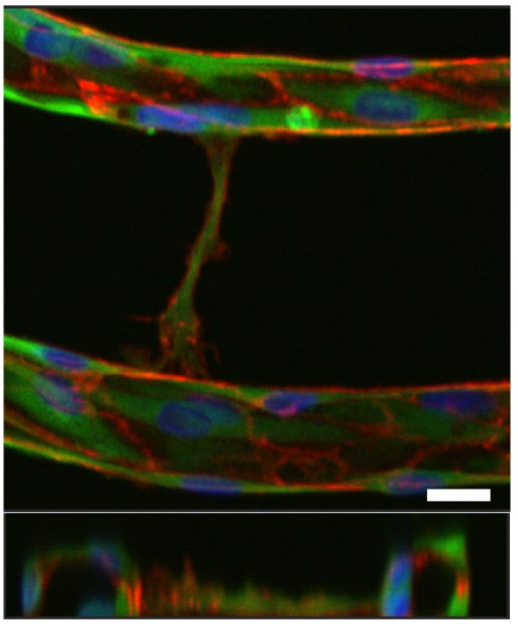

Figure S4: 3D-Sprout formation. *Sprout formation demonstrates the ability of ECs to modify the patterned hydrogel. Scalebar 10 µm*